Cell Reports

Synchronization of behavioral and cardiac dynamics in larval zebrafish

Graphical abstract

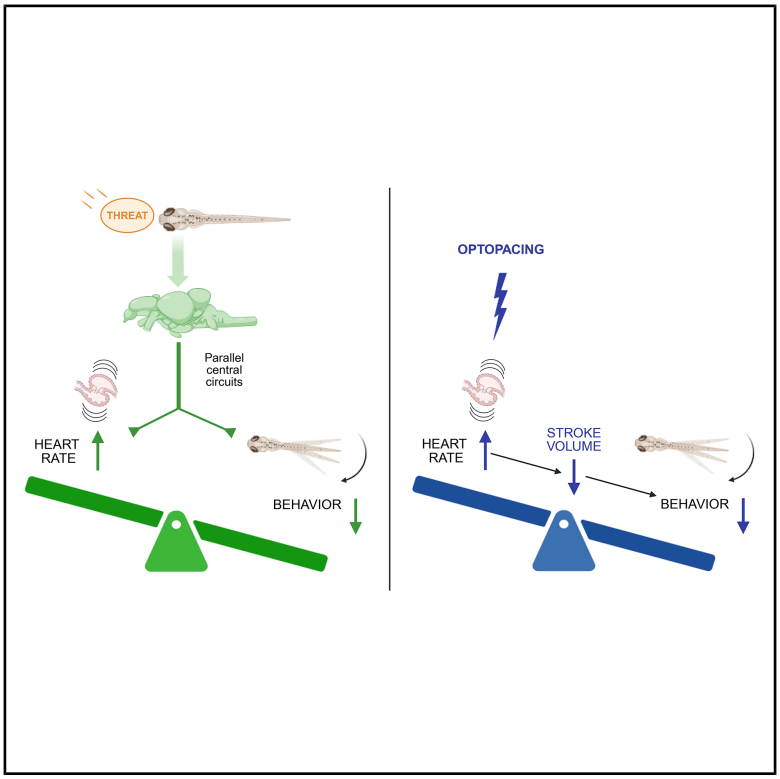

Highlights

- Threats lead to a coupled tachycardia and behavioral state in larval zebrafish
- Neural dynamics across the brain and autonomic nervous system reflect this state
- Interoception is not required for this coupling
- Optically pacing the heart also suppresses OMR but by reducing blood flow

Authors

Kristian J. Herrera, Arman Zarghani-Shiraz, Misha B. Ahrens, Florian Engert, Mark C. Fishman

Correspondence

mark_fishman@harvard.edu

In brief

Herrera et al. show that in larval zebrafish, heart rate and engagement in the optomotor response are inversely related following threat. This synchronization emerges via parallel central mechanisms. Directly optopacing the heart also reduces visuomotor engagement but through alternative mechanisms related to reducing blood flow.

Herrera et al., 2026, Cell Reports *45*, 116947
February 24, 2026
https://doi.org/10.1016/j.celrep.2026.116947

CellPress

Cell Reports

CellPress
OPEN ACCESS

Report

Synchronization of behavioral and cardiac dynamics in larval zebrafish

Kristian J. Herrera,[1,2] Arman Zarghani-Shiraz,[1] Misha B. Ahrens,[3] Florian Engert,[2] and Mark C. Fishman[1,4,*]
[1]Harvard Department of Stem Cell and Regenerative Biology, Harvard University, Cambridge, MA 02138, USA
[2]Department of Molecular and Cellular Biology, Harvard University, Cambridge, MA 02138, USA
[3]Janelia Research Campus, Howard Hughes Medical Institute, Ashburn, VA 20147, USA
[4]Lead contact
*Correspondence: mark_fishman@harvard.edu
https://doi.org/10.1016/j.celrep.2026.116947

SUMMARY

Animals reprioritize behavioral goals in response to internal physiological states. Using larval zebrafish, we investigated whether engagement with a visuomotor task, the optomotor response (OMR), is coupled to cardiac dynamics. We discovered that threats lead to tachycardia that is synchronized with behavioral suppression. The change in heart rate is represented in the activity of specific neuronal populations. Severing the input to the sympathetic ganglia or ablating the vagus nerve revealed that the threat-related changes to behavioral state do not require interoceptive pathways. Direct tachycardic optopacing of the heart similarly suppressed the OMR response, but by reducing cardiac filling during diastole, thereby impacting oxygen delivery to the CNS. Optopacing also changed the activity of specific brain regions but in neurons distinct from those associated with threat-induced tachycardia. These cardiac function-associated central changes may have relevance to autonomic imbalances in anxiety, stress, and orthostatic disorders.

INTRODUCTION

Animals, including humans, couple their behaviors to physiological dynamics as a way to ensure actions support the internal needs of the body. For the cardiovascular system, heart rate and stroke volume of each beat are adjusted to ensure adequate oxygen delivery for central nervous system function and motor behaviors. This is accomplished via interoception[1] for chemicals and vascular stretch, sending afferent information via the vagus and glossopharyngeal nerves to brainstem neurons in the area postrema and the nucleus tractus solitarius.[2] These afferent signals guide motor output through the sympathetic and parasympathetic nerves to adjust heart rate, stroke volume, and vascular tone. Superimposed on this reflex arc is information from higher brain centers that helps to coordinate an integrated output. These physiological changes to threat responses are often associated with changes in brain function, for example, a sense of anxiety.

This synchrony of behavior, physiological function, and emotional state, has raised the possibility that physiological changes may cause alterations in emotional state, the so-called James-Lange model.[3] Indeed, it is known that various types of dysautonomia are associated with cognitive dysfunction, such as "brain fog" of unknown etiology, and direct perturbation of cardiac dynamics by optogenetics in mice can cause an anxiety-like state.[4] These observations suggest that alterations in cardiac function may change behaviors. However, whether this manipulation recapitulates the interoceptive representations generated during natural periods of tachycardia or is its own unique stimulus is still unclear.

Resolving this question requires combining visceral recording or manipulation in task-performing animals while monitoring the neural representations of internal states. Here, we use the larval zebrafish to address this challenge. In behaving fish, we can employ non-invasive, entirely optical methods to quantify visceral dynamics, behavior, and to monitor and manipulate the activity of neurons in the peripheral ganglia and central nervous systems. Although some high-order forebrain areas like the insular cortex are ill-defined in teleosts, even the developing larva possesses most of the key elements of the interoceptive network, including the bidirectional sympathetic and vagal paths of the autonomic nervous system,[5–7] suggesting that principles found in this model may translate across vertebrates.[8,9]

We focused on exploring how changes in cardiovascular physiology are integrated with the optomotor response (OMR), a robust behavior where the fish turns to follow whole field motion stimuli. Recently, we have shown that larvae can transition between states of engagement and disengagement with the OMR[10] but it is unknown what cues might trigger or represent these states. Further, the circuitry governing the optomotor response is well studied from sensory input to motor output.[11–19] Thus, by identifying how visceral activity is coordinated with this well-characterized neural transformation, we hope to open the door for further mechanistic dissections of the cells and circuits that unite body and behavior.

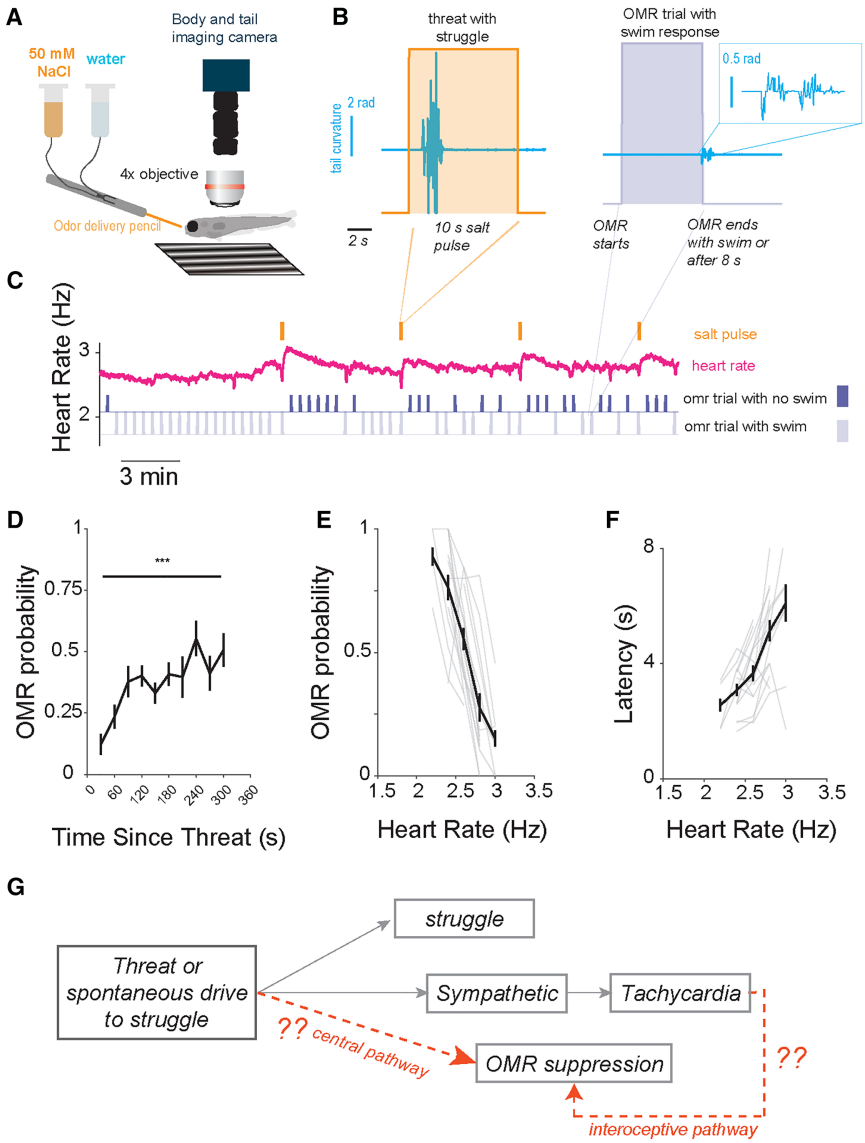

Figure 1. OMR rate is attenuated during tachycardia

(A) Schematic cartoon of experimental rig for recording tail and heart activity moving gratings (optometer response [OMR]) and salt-pulses via the odor delivery pencil.

(B) Example data collected from the tail (blue) during threat versus during OMR trials. During salt pulses, the fish tail responds with more rigorous (high cumulative tail angle) swims, aka "struggles," compared to the routine swims during the OMR trials. Inset from OMR trial shows tail deflections during the swim.

(C) Sample experiment where heart-rate is recorded (red) while observing the fish's tail (blue) respond (solid lines) or not (dashed lines) to optomotor trials interspersed with salt pulses (orange).

(D) Probability of detecting a swim during an OMR trial as a function of time since the most recent salt pulse ($n = 17$, $p = 0.0004$, paired t test). Error bars are SEM.

(E) Probability to respond to OMR during an 8-s whole-field motion trial as a function of heart rate immediately preceding the trial. Light gray lines indicate individual fish ($n = 17$). Error bars are SEM.

(F) Among trials where the fish swims, response time or latency is plotted as a function of heart rate. Light gray lines indicate individual fish ($n = 17$). Error bars are SEM.

(G) Schematic illustrating two alternative neural pathways, a central pathway or an interoceptive pathway that could synchronize tachycardia and OMR suppression.

RESULTS

Zebrafish alter cardiodynamics following threats

To test whether larval zebrafish couple cardiodynamics and behavioral state, we first aimed to establish a paradigm for eliciting robust changes in heart rate while monitoring tail motion. We modified a previously described preparation[20] for tail tracking and stimulating unanesthetized larvae immobilized in agarose to capture heart and tail motion through a single camera placed below the animal (Figure 1A). From this preparation, we visualize heartbeats as fluctuating luminances, or optical densities, enabling the extraction of the heart rate. From this information, we can also estimate relative stroke volume dynamics during each heartbeat (Figure S2), which are slightly anti-correlated with heart rate (Figures S2B and S2C).

In selecting stimuli, we reasoned that cues leading to high-energy behaviors might modulate internal state and heart rate.[21] Thus, we tested two stimuli, a visual "dark flash" and a chemical "salt pulse" that elicit struggles in head-embedded larvae[20,22] (Figure S1A). We find that while larvae are inactive during interstimulus periods, they often perform struggles, defined by high velocity bidirectional changes in the tail's curvature, within seconds of the onset of either cue (Figures S1B–S1D). These struggles are accompanied by an increase in heart rate, which otherwise is stable during the interstimulus periods. The cardiac response sometimes begins with a brief bradycardia, which is followed by a persistent tachycardia that builds over 15 to 20 s before decaying back to baseline after at least a minute (Figures S1B–S1D). When threats fail to induce a struggle, no cardiac modulation occurs (Figures S1E and S1F). By contrast, spontaneous struggles are followed by a tachycardia state (Figure S1G), and 95% of all tachycardia events begin within 10 s of a struggle (Figure S1H), suggesting that the observed tachycardia is coupled to high-energy locomotor output rather than the tested stimuli.

Zebrafish larvae are less responsive to whole-field motion (OMR) during tachycardia

We explored whether threat-related changes in heart rate are associated with changes in the OMR, in which the fish is shown

a pattern of moving stripes and responds by turning its tail in the direction of movement. We compared the number of times the fish performed the OMR depending on heart rate (Figures 1B and 1C). We found that threat-induced (Figures 1D and 1E) as well as spontaneous tachycardia (Figure S1H) is associated with a marked decrease in responsive OMR trials. Among OMR trials, when the larvae did respond, tachycardia was also associated with a longer response latency (Figure 1F). During these trials, the probability of turning with the direction of the moving stripes is independent of heart rate, indicating that they are still engaging with the stimulus (Figure S1I). In addition to changes in the OMR, the response rate to dark flashes is lower at higher heart rates (Figure S1J). These data indicate that, following a struggle, a brain state with suppressed motor responses is synchronized with the tachycardia (Figure 1G).

Distributed neural populations in the brain reflect heart rate

The presence of a coupled cardiac-behavioral state indicates that there should be activity in the brain that fluctuates alongside heart rate. To identify these regions, we used two-photon imaging of calcium activity of larvae being exposed to tachycardia-generating threats (Figure 2B). In particular, using *tg(vGlut2a:gal4;uas:GCaMP6S)*[23] fish, we imaged the activity of glutamatergic neurons across the brain, which we registered to the Z-brain atlas[24] in order to map the activity to specific brain regions (Figures 2B and S4). We observed cells in specific regions whose activity is either strongly correlated or strongly anti-correlated with heart rate (Figure 2B). During tachycardia, more regions, including parts of the pallium, thalamus, habenula, and inferior olive, have suppressed neural activity (Figure 2C). Most prominent is a thalamic structure "mesencephalic-vGlut-cluster 1" that has been thought homologous to the Edinger-Westphal nucleus that regulates response latencies and arousal states.[21] Among the areas with increased activity during tachycardia are the habenula, pineal gland, and the area postrema.

Sympathetic manipulation suggests that threat independently affects cardiac and behavioral states

Are these behavioral and neural states downstream of the visceral dynamics, as speculated in the James-Lange model, or are they downstream of shared central control (Figure 1G)? Central mediation of threat-induced tachycardia is likely via sympathetic activation. We confirmed this by calcium imaging in transgenic fish that express a calcium indicator in noradrenergic (and dopaminergic) neurons (*tg(Th1:gal4; UAS:GCaMP6f)*)[25] (Figures 3A and 3B). These experiments revealed that across both bilateral pairs of sympathetic ganglia, nearly every sympathetic neuron imaged has dynamics that are highly correlated (>0.5) with heart rate across the entire imaging session, whether at rest or under threat (Figures 3C and 3D). The brief post-threat bradycardia, however, is absent from sympathetic dynamics and instead corresponds to transient activation of a subset of heart-rate-encoding cholinergic[26] vagal motor neurons (Figure S5). Given the brevity of this bradycardia, we focused on subsequent manipulations on sympathetic signaling.

If the tachycardia, per se, was responsible for OMR suppression, then direct sympathetic activation should drive both tachycardia and OMR suppression. To test this, we optogenetically excited the noradrenergic neurons of transgenic fish expressing the channelrhodopsin variant from *Chloromonas oogama* (CoChR) in cells that produce dopamine-β-hydroxylase, a norepinephrine precursor (Figure 3E). At baseline, these fish behave similarly to controls (Figures S6A and S6B). We observed that brief illumination from a blue LED induced a persistent (90 s) tachycardia in CoChR-expressing fish (Figure 3F), without inducing struggles (Figure S6C). During this optogenetically induced tachycardia, the larvae's likelihood to perform the OMR is significantly reduced (Figure 3G) but not for control fish exposed to blue light. Across control and CoChR-expressing fish, heart rate and the OMR occupy the same overall relationship (Figures S6D and S6E), suggesting a contribution of sympathetic-induced tachycardia to OMR suppression. However, we cannot sufficiently spatially constrain the region activated by blue light to rule out co-activation of hindbrain noradrenergic centers alongside the sympathetic ganglia.[18]

We next wanted to test whether blocking the subset of noradrenergic receptors that mediate heart rate increases is also sufficient to reduce engagement with the OMR. Blocking β-adrenergic receptor activation with propranolol (Figure S6F) leads to a 55% reduction in the average baseline heart rate (Figure S6G), accompanied by a 40% increase in baseline OMR probability (Figure S6H). Stressors continue to generate struggles but the subsequent tachycardia is blunted by 40% (Figure S6I), while behavioral suppression is attenuated (Figure S6J). Meanwhile, the residual variation in heart rate is still predictive of OMR probability and latency (Figures S6J and S6K). Interestingly, neuronal activity in the sympathetic ganglia following a struggle is, itself, reduced by propranolol (Figure S6L), indicating that the drug also acts on circuits upstream of the sympathetic ganglia.

These sets of experiments suggest that both tachycardia and behavioral states are modulated by noradrenergic signaling. However, neither manipulation distinguishes whether both cardiac and behavioral changes follow the peripheral action of the sympathetic ganglia or via separate noradrenergic populations. To pinpoint the effects of the peripheral sympathetic ganglia, we used a two-photon laser to sever the cholinergic preganglionic input from the spinal cord to the sympathetic ganglia (Figure 3H). Following this manipulation, baseline heart rate and OMR were unaffected (Figures S9A and S9B) as was the propensity to struggle during threats (Figure S9C). However, the zebrafish no longer increased their heart rate following a threat (Figure 3I). Despite the absence of tachycardia, OMR responsiveness still dramatically drops following a threat and recovers back to baseline with similar dynamics as sham ablations (Figures 3J and 3K). These results indicate that heart rate changes are not necessary for the reduction in OMR. Instead, the simplest explanation is that heart rate and OMR are regulated in parallel, presumably from higher-order CNS neurons.

If coordination of heart rate and OMR occurs through "top-down" orchestration by the brain, then removal of "bottom-up" signals from the body should not affect the correlation. To test this prediction, we used a two-photon laser to sever both the left and right vagus nerve dorsal to the nodose ganglia (Figure 4A). We saw no difference between ablated fish and controls in how engagement with the OMR correlates with heart rate

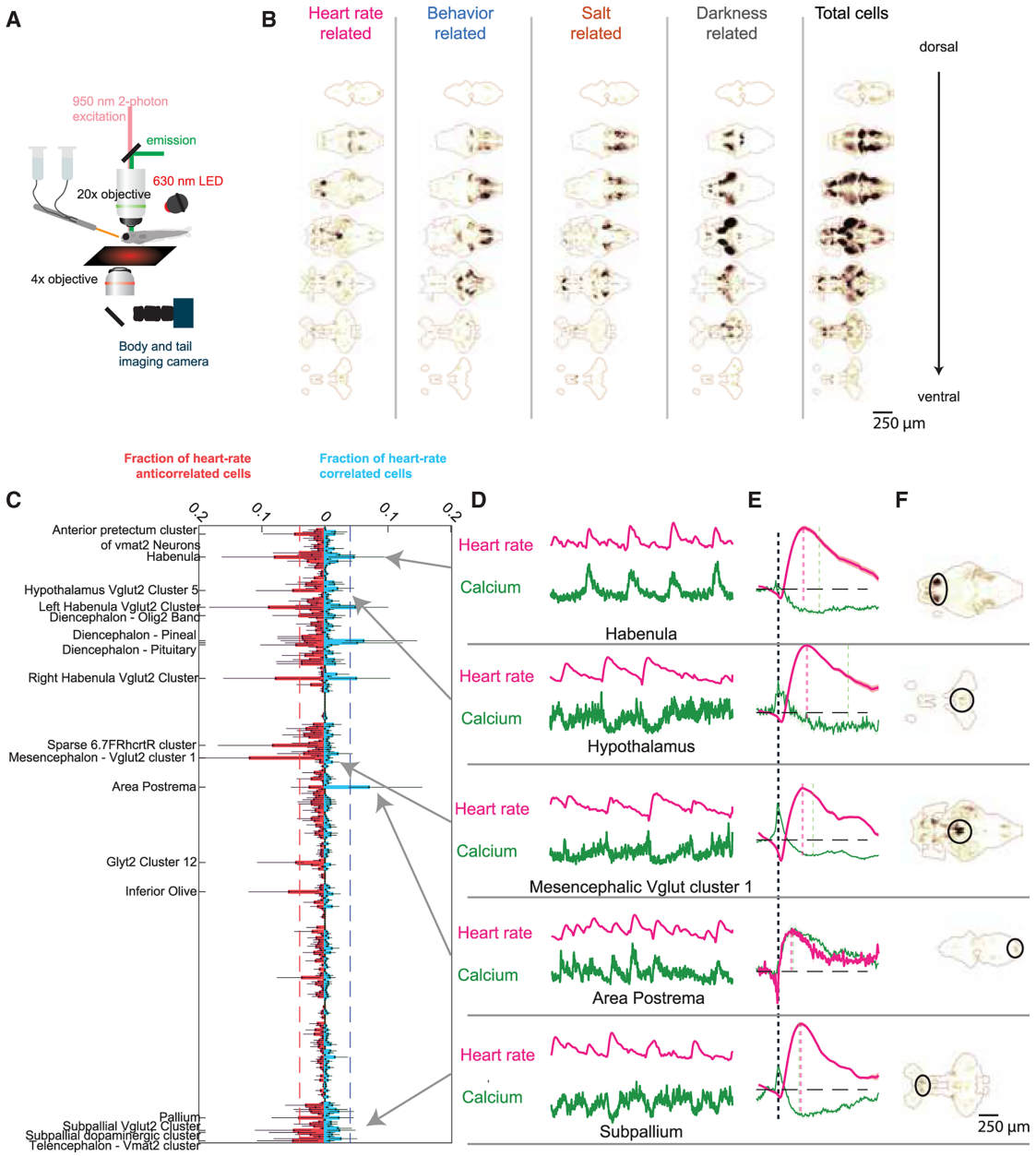

Figure 2. Cardiac state is encoded in neural dynamics across distributed brain regions

(A) Schematic cartoon of experimental rig for imaging the brain, tail, and heart, while also presenting dark flashes (via the red LED) and salt-pulses via the odor delivery pencil.

(B) Brain-wide maps of all recorded neurons across tg(vglut2a:gal4;uas:GCaMP6S) fish registered to the Z-brain atlas, heart-rate-correlated neurons, as well as behavior, salt, and dark flash correlated neurons (scale bar 250 µm).

(C) Fraction of significant heart rate correlated (blue, right) and anti-correlated (red, left) cells in every Z-brain demarcated mask. Labeled masks are those containing the highest fraction of heart-rate encoding cells (>5% of cells are either correlated ($r > 0.3$) or anti-correlated ($r < -0.3$). Error bars indicate 95% confidence interval.

(D) Sample heart rate and calcium activity traces from representative cells in the area postrema, habenula, hypothalamus, mesencephalic-vGlut-cluster 1, and subpallium.

(E) Struggle-triggered average of heart rate and calcium dynamics from heart-rate correlated cells in the areas indicated in (D).

(F) Anatomical location in (B) of the regions depicted in (D and E). Scale bars, 250 µm.

CellPress
OPEN ACCESS

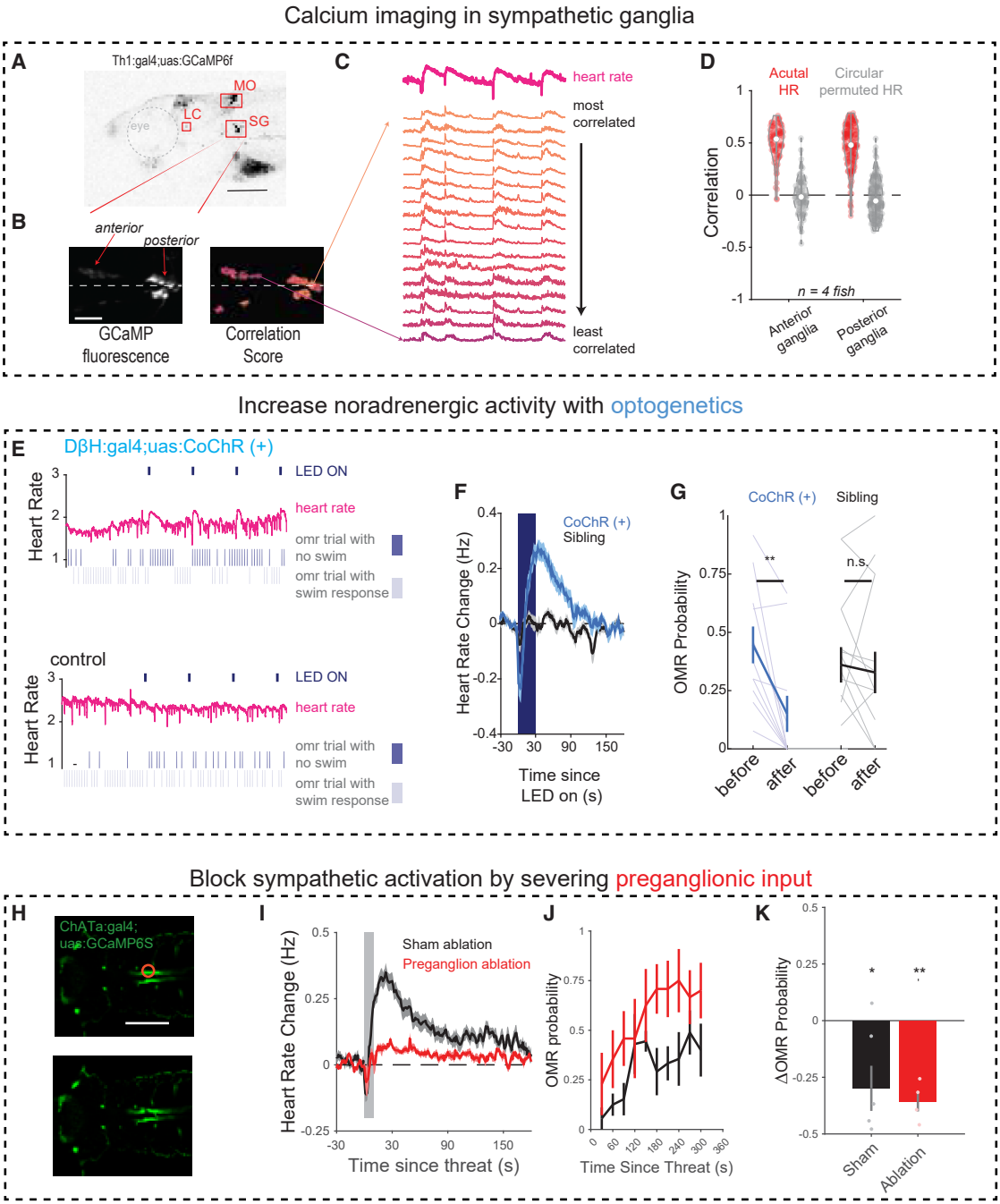

Figure 3. Noradrenergic signaling encodes and regulates cardio-behavioral state

(A) Projection of confocal stack of tg(th1:gal4;uas:GCaMP6f) fish imaged from the side. A dashed circle indicates the eye. Scale bars, 150 μm.

(B) Dorsal view of a two-photon image of the sympathetic ganglia anatomy (left) and correlation score with heart rate for each cell's calcium signal overlaid on top (right) and indicated by color. Scale bars, 30 μm.

(C) Heart rate and calcium traces from (B) sorted by correlation score.

(D) Correlation of all sympathetic neurons in the anterior (left) and posterior (right) ganglia to the recorded heart rate (red) and circularly permuted heart rate signal (gray).

(E) Sample experiment recording heart rate and OMR performance while optogenetically activating noradrenergic neurons (blue bars at top) in a tg(DβH:gal4;uas:CoChR-eGFP fish) (top) and an eGFP(−) sibling control fish (bottom).

(F) Heart rate change elicited by blue light exposure to tg(DβH:gal4;uas:CoChR-eGFP) fish (blue, $p = 0.00011$, paired t test, $n = 10$) and an eGFP(−) sibling control fish (gray, $p = 0.5837$, paired t test, $n = 11$). Shaded indicates SEM.

(legend continued on next page)

(Figures 4B–4E). Furthermore, we tested the removal of the area postrema, which, as a circumventricular organ, can act as an interoceptor,[27,28] but again saw no impact on the synchronization between heart rate and behavioral state (Figure S8). These results indicate that cardiac changes are not *necessary* to generate correlated behavioral states but do not rule out a potential causal role. Thus, we next sought to examine whether direct manipulation of cardiodynamics is *sufficient* to change the behavioral state of the animal.

Direct manipulation of cardiodynamics impacts the OMR through modulation of cardiac filling

To control cardiac rhythm directly, we employed optopacing, a technique previously demonstrated in zebrafish[29,30] and mice.[4] We expressed CoChR in cardiomyocytes (*myl7*) and used timed illumination to pace the heart at defined frequencies (Figures 4B and 4C). We selected two target heart rates—2 (Figure 4D) and 2.5 Hz (Figure 4E)—which resemble baseline and threat-evoked tachycardia, respectively. Control larvae exposed to this light stimulation show no behavioral effects (Figure 4F). By contrast, in fish expressing CoChR, this pacing has strong effects on their behavior. In fact, even pacing at 2 Hz diminished the OMR response, while increasing the rate of stimulation suppressed it further (Figure 4G).

The reduction in OMR by optogenetic stimulation at baseline rates suggests that the optogenetic technique might have non-chronotropic cardiovascular effects. For example, optopacing may reduce the volume ejected with each beat (stroke volume) compared to normal beats. We inferred relative stroke volume from optical density changes and observed that, compared to the unpaced heart, the ventricle of the paced heart fills less during diastole (Figures S9A–S9C). This was true at both 2 and 2.5 Hz, and the magnitude (10%–20%) was notably higher than seen following a threat (~5%, Figure S1D). By changing the duration of the LED pulse, we could test the effects of the ratio of time spent in diastole to systole, where less time spent in diastole means less filling time for the ventricle, and a lower output in the next beat. We found that even at the same heart rate (2 Hz), a decreased diastole time leads to reduced OMR rate (Figures S9F and S9G), suggesting that decreases in stroke volume during pacing are largely responsible for suppressing the OMR.

Reduction in blood flow to the brain diminishes oxygen delivery and neural function. Therefore, we tested the effects of providing supplemental (70%) oxygen and found that this reduced the pacing-induced diminution in OMR (Figure 4H). By contrast, the threat-induced reduction of OMR persists in hyperoxia (Figure 4I). Thus, we conclude that the mechanisms that drive behavioral suppression during optopacing are distinct from those accompanying tachycardia associated with threat and are more related to impaired oxygen delivery to the brain.

Natural tachycardia and optical pacing have distinct effects on interoceptive populations

The different physiological mechanisms by which optopacing and environmental threats suppress the OMR suggest that their sensory representations are different. To test this supposition, we imaged neuronal activity in putative interoceptive regions, the vagal ganglia, and area postrema, using *tg(vGlut2a:gal4;UAS:GCaMP6s)*[23] fish. In the vagal ganglia (Figure 5A), we found primary sensory neurons across the different sensory ganglia with dynamics that correlate with heart rate (Figures 5B and 5C), as previously described.[31] However, with optopacing, these neurons did not respond (Figures 5D and 5E), indicating that the two forms of tachycardia are registered differently in the primary sensory neurons.

We also examined the area postrema, a circumventricular organ that may act as an interoceptor monitoring factors correlated with hemodynamics[27,28] and is the region we found to have the highest frequency of neurons positively correlated with heart rate in response to threat (Figure 2C).[27,28] We found that both modes of inducing tachycardia altered area postrema activity but in different populations of neurons (Figures 5F–5H). These data further support the notion that optopacing has a distinct sensory representation from the threat-related tachycardia.

DISCUSSION

This study set out to understand how animals coordinate their behavioral states with internal physiological dynamics. We focused on the linkage between cardiovascular dynamics and a specific visuomotor task, the OMR, and found that as heart rate increases, the OMR engagement decreases. The mechanism of the linkage, however, is different depending on how the tachycardia arises. Specifically, during threat, changes in heart rate can be dissociated from those in OMR, suggesting central parallel control of both. Optogenetic pacing, on the other hand, impairs cardiac output, which then contributes to behavioral suppression.

We found that direct optopacing of cardiomyocytes in the heart[4,29,32] reduces the OMR rate. However, this perturbation has a secondary hemodynamic effect, in which optically paced beats have reduced stroke volumes. We believe the pacing effect arises primarily from this impaired blood flow, as the effect of optopacing can be abrogated with hyperoxia. This effect parallels the sudden drops in blood pressure recorded during anxiogenic optopacing experiments in mice[4] and is reminiscent of the so-called "pacemaker syndrome" noted with ventricular-alone pacing in humans.[33] In such patients, the abnormal site of beat initiation from the ventricle rather than the sino-atrial node leads to reduced stroke volume, sometimes with

(G) Change in OMR rate between the 90 s before and 90 s after blue light exposure for tg(DβH:gal4;uas:CoChR-eGFP) fish (blue, $p = 0.002$, paired two-sided rank test, $n = 10$) and eGFP(−) sibling control fish (gray, $p = 0.4667$, paired two-sided rank test, $n = 11$). Lighter lines indicate individual fish. Error bars are SEM.
(H) Anatomy of cholinergic preganglionic nerves in the medial-ventral spinal cord before (top) and after (bottom) unilateral two-photon ablation. Scale bars, 150 μm.
(I) Change in heart rate after a salt pulse for neurons with sham (black) and preganglionic (red) ablations.
(J) OMR probability as a function of time since threat after sham (black) and preganglionic ablations (red). Error bars are SEM.
(K) Change in OMR probability before and after threat for fish with sham and preganglionic ablations ($p = 0.0301$ and $p = 0.004$, t test). Error bars are SEM.

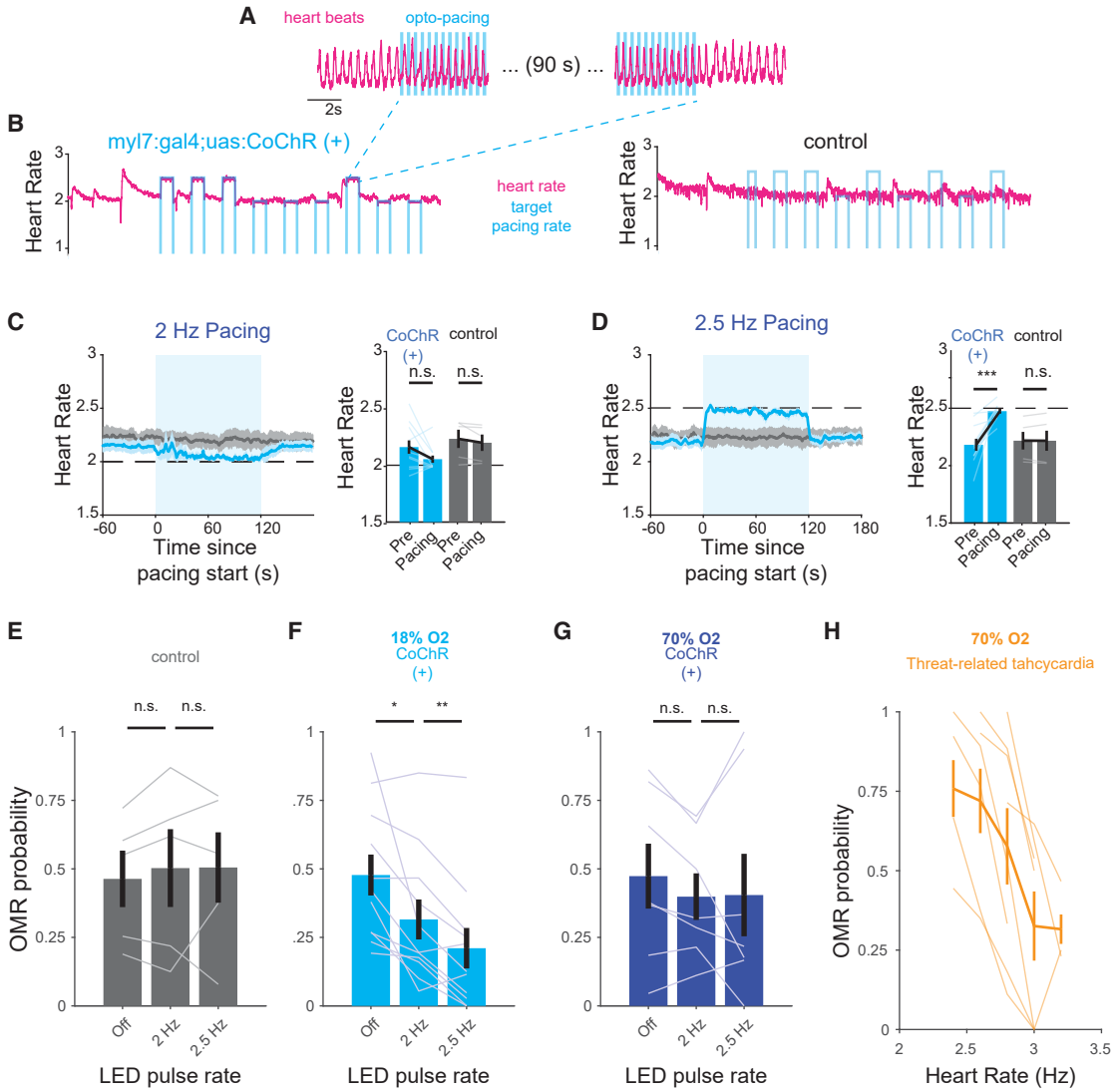

Figure 4. Optical pacing of heart rate suppresses OMR through oxygen-dependent mechanisms

(A) Heart beats 5 s before, during pacing (blue bars indicate where the blue light is on), and 5 s after pacing stops.

(B) Sample experiment recording heart rate while optogenetically pacing the heart to different target rates (2 or 2.5 Hz, blue line) in a tg(myl7:CoChR-tdTomato) fish (left) and a tdTomato sibling control fish (right).

(C) Left: average time course of heart rate centered on the onset of 2 Hz pacing for tg(myl7:CoChR-tdTomato) fish (blue) and tdTomato(−) sibling control fish (gray). The shaded area indicates SEM. Right: average heart rate before and during pacing for the same groups (blue: $p = 0.0003$; gray: $p = 0.977$, paired t test).

(D) Same as (C) but for 2.5 Hz pacing (blue: $p = 0.0726$; gray: $p = 0.2102$, paired t test).

(E) Relationship between optical pacing and probability to perform OMR in tdTomato(−) sibling controls (gray, $n = 5$, $p = 0.3712$ and $p = 0.9762$, paired t test) in normal oxygen conditions (18% O_2). Lighter lines indicate individual fish. Error bars are SEM.

(F) Relationship between optical pacing and probability to perform OMR in myl7:CoChR-tdTomato fish (blue, $n = 10$, $p = 0.0182$ and $p = 0.0030$, paired t test) in normal oxygen conditions (18% O_2). Lighter lines indicate individual fish. Error bars are SEM.

(G) Same as (F) but in hyperoxic conditions (70% O_2).

(H) Relationship between heart rate and OMR during threat-related tachycardia in hyperoxic conditions (70% O_2). Light lines indicate individual fish. Error bars are SEM.

accompanying confusion or other changes in brain state.[34–36] However, it is still unclear how the hemodynamic effects of opto-pacing alter the OMR. This may involve neurons, potentially in the area postrema, that are intrinsically sensitive to hemodynamic changes or non-neuronal cell types, such as endothelial[37] or glial cells[18] that detect and then relay this information to neurons. These cells may be responding to pulsatility, oxygen levels, or other factors that accumulate under low flow conditions, such as lactic acid or carbon dioxide.

The changes in motor behaviors alongside heart rate are surrogates for an altered brain state. The several mechanisms of this coupling are of interest as potential underpinnings of disorders

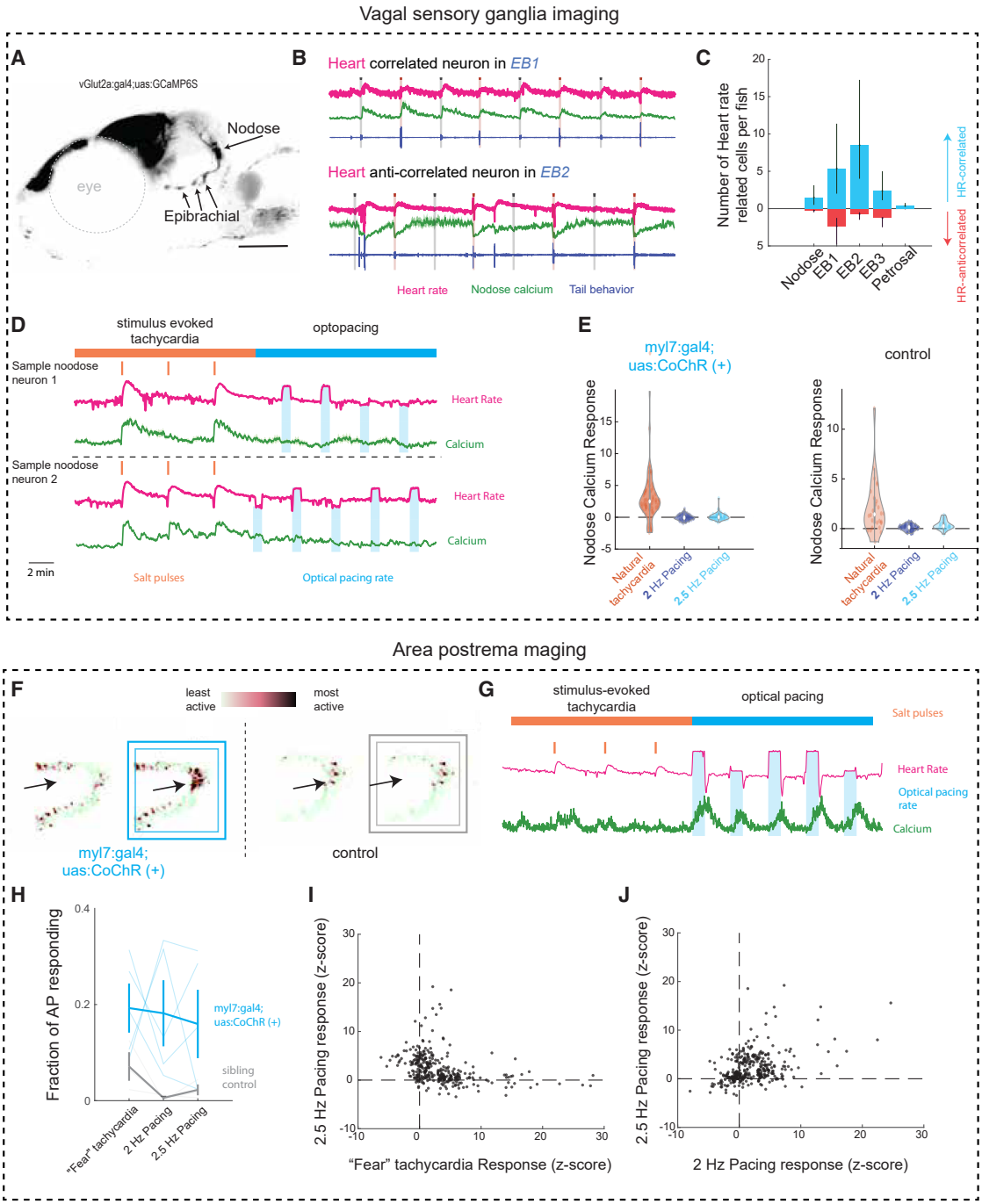

Figure 5. Interoceptive populations respond differently to threat-related tachycardia compared to optopaced changes in heart rate

(A) Projection of confocal stack of vGlut2a:gal4;uas:GCaMP6s fish imaged from the side. The eye is indicated by a dashed circle. Scale bars, 150 μm.

(B) Sample heart rate, behavior, and calcium activity traces recorded from heart rate correlated (top) and anti-correlated (bottom) cells from the epibrachial ganglia.

(C) Median number of heart rate correlated ($r > 0.3$, blue) and anti-correlated ($r < -0.3$, red) cells found in each ganglion (nodose, 3 epibrachial, and petrosal) across 8 fish. Error bars indicate 95% confidence intervals (1,000 bootstraps).

(D) Heart rate and calcium recordings from an experiment combining optopacing and calcium imaging in the nodose showing cells that are correlated with heart rate during "natural tachycardia" epoch and the responses of those cells during the 15 min optopacing period of 60 s of pacing separated by 120 s of rest.

(E) Violin plots of the activity of "natural heart-rate" correlated neurons following presentation of salt pulse (orange), 2 Hz pacing (dark blue), and 2.5 Hz pacing (light blue) for myl7:CoChR-tdTomato fish (left, $n = 4$ fish) and tdTomato(−) sibling controls (right, $n = 2$ fish).

(legend continued on next page)

marked by both autonomic dysfunction and cognitive disorders. Long COVID-19 and other post-viral infections often include problems with heart rate control (e.g., postural orthostatic tachycardia syndrome [POTS]) along with "brain fog." The mechanisms are not known, but in POTS, for example, the poor control of orthostatic blood pressure in some cases appears to be associated with centrally driven hyperadrenergic drive and others with reduced brain blood flow, analogous to the distinct causes for tachycardia-induced changes we have uncovered here.[38]

Limitations of the study

Clearly, there is a central contribution to threat-induced OMR changes and a diastolic filling component to the optomotor changes. We cannot rule out definitively that heart rate, per se, ever has a regulatory role. This might emerge or be easier to define in older embryos when the heart is more heavily innervated by afferent neurons. At this point, it also remains unclear what upstream threat-induced signal is used by the animal to drive the reduction in OMR. One possibility is noradrenergic signaling through astrocytes, which in zebrafish is known to trigger a passive, OMR-inattentive state.[18,39,40] Additionally, we find populations of heart rate anti-correlated neurons across the preoptic area of the hypothalamus and Edinger-Westphal nucleus, which are important for managing arousal,[21,41] energy homeostasis,[42,43] and the habenula, which, through its projections to the interpeduncular nucleus[44] and raphe,[45,46] is a critical hub for managing behavioral selection in fish and mammals.[47–49] Deciphering how these distributed neural populations interact will become feasible as connectomics efforts in the zebrafish reveal comprehensive wiring diagrams of the zebrafish brain.[50–53]

RESOURCE AVAILABILITY

Lead contact

Further information and questions or inquiries about data and resources should be directed to the lead contact, Mark C. Fishman (mark_fishman@harvard.edu).

Materials availability

All transgenic lines made in this study will be available on request.

Data and code availability

- Processed data are publicly available at https://doi.org/10.5281/zenodo.18135842. Any additional raw data can be provided upon request.
- Original analysis code is publicly available and provided at https://doi.org/10.5281/zenodo.18135842 as well as https://github.com/kjherrera23/Herrera2026CardiacBehaviorSynch
- Any additional information required to reanalyze the data reported in this paper is available from the lead contact or kjherrera23@gmail.com upon request.

ACKNOWLEDGMENTS

This study was supported by NIH grants U19NS104653 and 1R01NS124017 to F.E. and M.C.F., Howard Hughes Medical Institute to M.B.A., and Simons Foundation SCGB 542943SPI to F.E. and M.B.A. We thank the Harvard Center for Biological Imaging (RRID: SCR018673) for infrastructure and support. We thank the Janelia Visiting Scientist Program for support. We thank all members of the Fishman, Engert, and Ahrens laboratories and Adrienne Fairhall for feedback over the course of this project. We would also like to thank Niko Hoerrmann for feedback on the manuscript.

AUTHOR CONTRIBUTIONS

Conceptualization, K.J.H., M.C.F., and F.E.; methodology, K.J.H. and A.Z.-S.; investigation, K.J.H.; visualization, K.J.H.; writing – original draft, K.J.H. and M.C.F.; writing – review & editing, K.J.H., F.E., and M.C.F.; funding acquisition, M.B.A., F.E., and M.C.F.; project administration, F.E. and M.C.F.; and supervision, M.B.A., F.E., and M.C.F.

DECLARATION OF INTERESTS

The authors declare no competing interests.

STAR★METHODS

Detailed methods are provided in the online version of this paper and include the following:

- KEY RESOURCES TABLE
- EXPERIMENTAL MODEL AND STUDY PARTICIPANT DETAILS
  - Animal husbandry
- METHOD DETAILS
  - Transgenic line generation
  - Heart rate and behavior acquisition
  - Whole field motion stimulation
  - Pharmacology
  - Calcium imaging
  - Optogenetic cardiac pacing experiments
  - 2-Photon ablations
- QUANTIFICATION AND STATISTICAL ANALYSIS
  - Extraction of heart rate and relative fill volume from saved images
  - Image segmentation and registration
  - Identification of heart-rate related cells

SUPPLEMENTAL INFORMATION

Supplemental information can be found online at https://doi.org/10.1016/j.celrep.2026.116947.

Received: May 6, 2025
Revised: November 3, 2025
Accepted: January 8, 2026
Published: February 3, 2026

REFERENCES

1. Prescott, S.L., and Liberles, S.D. (2022). Internal senses of the vagus nerve. Neuron *110*, 579–599.

(F) Raw fluorescence of area postrema during baseline and pacing (squares) for CoChR-tdTomato (blue) and control fish (gray). Activity increases from light to dark.
(G) Same as (D) but from the area postrema.
(H) Fraction of area postrema that is active during pacing for CoChR-tdTomato (blue, $n = 5$) and control fish (gray, $n = 3$).
(I) Scatterplot of Z scores for area postrema cell response to salt response and 2.5 Hz pacing from area postrema cells that respond to one of the 3 stimuli.
(J) Same as (H) but comparing 2 and 2.5 Hz pacing.

2. Chen, W.G., Schloesser, D., Arensdorf, A.M., Simmons, J.M., Cui, C., Valentino, R., Gnadt, J.W., Nielsen, L., Hillaire-Clarke, C.S., Spruance, V., et al. (2021). The Emerging Science of Interoception: Sensing, Integrating, Interpreting, and Regulating Signals within the Self. Trends Neurosci. *44*, 3–16.
3. C.G. Lange and W. James, eds. The Emotions, *1* (Williams & Wilkins Co).
4. Hsueh, B., Chen, R., Jo, Y., Tang, D., Raffiee, M., Kim, Y.S., Inoue, M., Randles, S., Ramakrishnan, C., Patel, S., et al. (2023). Cardiogenic control of affective behavioural state. Nature *615*, 292–299.
5. Mann, K.D., Hoyt, C., Feldman, S., Blunt, L., Raymond, A., and Page-McCaw, P.S. (2010). Cardiac response to startle stimuli in larval zebrafish: sympathetic and parasympathetic components. Am. J. Physiol. Regul. Integr. Comp. Physiol. *298*, R1288–R1297.
6. Schwerte, T., Prem, C., Mairösl, A., and Pelster, B. (2006). Development of the sympatho-vagal balance in the cardiovascular system in zebrafish (Danio rerio) characterized by power spectrum and classical signal analysis. J. Exp. Biol. *209*, 1093–1100.
7. Stoyek, M.R., Croll, R.P., and Smith, F.M. (2015). Intrinsic and extrinsic innervation of the heart in zebrafish (Danio rerio). J. Comp. Neurol. *523*, 1683–1700.
8. Stoyek, M.R., MacDonald, E.A., Mantifel, M., Baillie, J.S., Selig, B.M., Croll, R.P., Smith, F.M., and Quinn, T.A. (2022). Drivers of sinoatrial node automaticity in zebrafish: Comparison with mechanisms of mammalian pacemaker function. Front. Physiol. *13*, 818122.
9. Stoyek, M.R., Quinn, T.A., Croll, R.P., and Smith, F.M. (2016). Zebrafish heart as a model to study the integrative autonomic control of pacemaker function. Am. J. Physiol. Heart Circ. Physiol. *311*, H676–H688.
10. Krishnan, K., Muthukumar, A., Sterrett, S., Pflitsch, P., Fairhall, A.L., Fishman, M., Bahl, A., Zwaka, H., and Engert, F. (2025). Attentional switching in larval zebrafish. Sci. Adv. *11*, eads4994.
11. Baier, H., and Wullimann, M.F. (2021). Anatomy and function of retinorecipient arborization fields in zebrafish. J. Comp. Neurol. *529*, 3454–3476.
12. Kramer, A., Wu, Y., Baier, H., and Kubo, F. (2019). Neuronal architecture of a visual center that processes optic flow. Neuron *103*, 118–132.e7.
13. Kubo, F., Hablitzel, B., Dal Maschio, M., Driever, W., Baier, H., and Arrenberg, A.B. (2014). Functional architecture of an optic flow-responsive area that drives horizontal eye movements in zebrafish. Neuron *81*, 1344–1359.
14. Naumann, E.A., Fitzgerald, J.E., Dunn, T.W., Rihel, J., Sompolinsky, H., and Engert, F. (2016). From Whole-Brain Data to Functional Circuit Models: The Zebrafish Optomotor Response. Cell *167*, 947–960.e20.
15. Dragomir, E.I., Štih, V., and Portugues, R. (2020). Evidence accumulation during a sensorimotor decision task revealed by whole-brain imaging. Nat. Neurosci. *23*, 85–93.
16. Bahl, A., and Engert, F. (2020). Neural circuits for evidence accumulation and decision making in larval zebrafish. Nat. Neurosci. *23*, 94–102.
17. Markov, D.A., Petrucco, L., Kist, A.M., and Portugues, R. (2021). A cerebellar internal model calibrates a feedback controller involved in sensorimotor control. Nat. Commun. *12*, 6694.
18. Mu, Y., Bennett, D.V., Rubinov, M., Narayan, S., Yang, C.-T., Tanimoto, M., Mensh, B.D., Looger, L.L., and Ahrens, M.B. (2019). Glia Accumulate Evidence that Actions Are Futile and Suppress Unsuccessful Behavior. Cell *178*, 27–43.e19.
19. Kawashima, T., Zwart, M.F., Yang, C.-T., Mensh, B.D., and Ahrens, M.B. (2016). The Serotonergic System Tracks the Outcomes of Actions to Mediate Short-Term Motor Learning. Cell *167*, 933–946.e20.
20. Herrera, K.J., Panier, T., Guggiana-Nilo, D., and Engert, F. (2021). Larval Zebrafish Use Olfactory Detection of Sodium and Chloride to Avoid Salt Water. Curr. Biol. *31*, 782–793.e3.
21. Lovett-Barron, M., Andalman, A.S., Allen, W.E., Vesuna, S., Kauvar, I., Burns, V.M., and Deisseroth, K. (2017). Ancestral Circuits for the Coordinated Modulation of Brain State. Cell *171*, 1411–1423.e17.
22. Lamiré, L.A., Haesemeyer, M., Engert, F., Granato, M., and Randlett, O. (2023). Functional and pharmacological analyses of visual habituation learning in larval zebrafish. eLife *12*, RP84926. https://doi.org/10.7554/eLife.84926.
23. Satou, C., Kimura, Y., Hirata, H., Suster, M.L., Kawakami, K., and Higashijima, S.-I. (2013). Transgenic tools to characterize neuronal properties of discrete populations of zebrafish neurons. Development *140*, 3927–3931.
24. Randlett, O., Wee, C.L., Naumann, E.A., Nnaemeka, O., Schoppik, D., Fitzgerald, J.E., Portugues, R., Lacoste, A.M.B., Riegler, C., Engert, F., and Schier, A.F. (2015). Whole-brain activity mapping onto a zebrafish brain atlas. Nat. Methods *12*, 1039–1046.
25. Li, J., Zhang, B.-B., Ren, Y.-G., Gu, S.-Y., Xiang, Y.-H., and Du, J.-L. (2015). Intron targeting-mediated and endogenous gene integrity-maintaining knockin in zebrafish using the CRISPR/Cas9 system. Cell Res. *25*, 634–637.
26. Förster, D., Arnold-Ammer, I., Laurell, E., Barker, A.J., Fernandes, A.M., Finger-Baier, K., Filosa, A., Helmbrecht, T.O., Kölsch, Y., Kühn, E., et al. (2017). Genetic targeting and anatomical registration of neuronal populations in the zebrafish brain with a new set of BAC transgenic tools. Sci. Rep. *7*, 5230.
27. Ferrario, C.M., Barnes, K.L., Szilagyi, J.E., and Brosnihan, K.B. (1979). Physiological and pharmacological characterization of the area postrema pressor pathways in the normal dog. Hypertension *1*, 235–245.
28. Fink, G.D., Bruner, C.A., and Mangiapane, M.L. (1987). Area postrema is critical for angiotensin-induced hypertension in rats. Hypertension *9*, 355–361.
29. Arrenberg, A.B., Stainier, D.Y.R., Baier, H., and Huisken, J. (2010). Optogenetic control of cardiac function. Science *330*, 971–974.
30. Savoie, E., Ramadan, A., Purvis, K., Stoyek, M., and Quinn, A. (2024). A Non-invasive In Vivo Experimental Model of Heart Failure Using Optogenetic Tachypacing in Larval Zebrafish. Circulation *150*, A4139898.
31. Hernandez-Nunez, L., Avrami, J., Shi, S., Markarian, A., Kim, A., Boulanger-Weill, J., Rutten, V., Zarghani-Shiraz, A., Ahrens, M., Engert, F., and Fishman, M.C. (2025). Emergence of functional heart-brain circuits in a vertebrate. Preprint at. eLife. https://doi.org/10.7554/eLife.109362.1.sa3.
32. Baillie, J.S., Stoyek, M.R., and Quinn, T.A. (2021). Seeing the light: The use of zebrafish for optogenetic studies of the heart. Front. Physiol. *12*, 748570.
33. Özmen, M., Altunkaya, O., Aydemir, S., Aydın, S.Ş., Aydınyılmaz, F., Aksakal, E., and Alkan, E. (2025). Evaluatıon of depressıon and anxıety status in patıents after cardıac devıce implantatıon. Ann. Noninvasive Electrocardiol. *30*, e70085.
34. Link, M.S., Hellkamp, A.S., and Estes, N.A.M. (2004). High incidence of pacemaker syndrome in patients with sinus node dysfunction treated with ventricular-based pacing in the mode selection trial (MOST). ACC Curr. J. Rev. *13*, 47–48.
35. Ellenbogen, K.A., Gilligan, D.M., Wood, M.A., Morillo, C., and Barold, S.S. (1997). The pacemaker syndrome – a matter of definition. Am. J. Cardiol. *79*, 1226–1229.
36. Ellenbogen, K.A., Thames, M.D., and Mohanty, P.K. (1990). New insights into pacemaker syndrome gained from hemodynamic, humoral and vascular responses during ventriculo-atrial pacing. Am. J. Cardiol. *65*, 53–59.
37. Jia, B.Z., Tang, X., Rossmann, M.P., Zon, L.I., Engert, F., and Cohen, A.E. (2025). Swimming motions evoke Ca2+ events in vascular endothelial cells of larval zebrafish via mechanical activation of Piezo1. Preprint at Current Biology. *35*, 6137–6146.e5. https://doi.org/10.1016/j.cub.2025.10.053.
38. Benarroch, E.E. (2012). Postural tachycardia syndrome: a heterogeneous and multifactorial disorder. Mayo Clin. Proc. *87*, 1214–1225.
39. Chen, A.B., Duque, M., Rymbek, A., Dhanasekar, M., Wang, V.M., Mi, X., Tocquer, L., Narayan, S., Legorreta, E.M., Eddison, M., et al. (2025).

Norepinephrine changes behavioral state through astroglial purinergic signaling. Science *388*, 769–775.

40. Duque, M., Chen, A.B., Hsu, E., Narayan, S., Rymbek, A., Begum, S., Saher, G., Cohen, A.E., Olson, D.E., Li, Y., et al. (2025). Ketamine induces plasticity in a norepinephrine-astroglial circuit to promote behavioral perseverance. Neuron *113*, 426–443.e5.
41. Reitz, S.L., and Kelz, M.B. (2021). Preoptic area modulation of arousal in natural and drug induced unconscious states. Front. Neurosci. *15*, 644330.
42. Akash, G., Kaniganti, T., Tiwari, N.K., Subhedar, N.K., and Ghose, A. (2014). Differential distribution and energy status-dependent regulation of the four CART neuropeptide genes in the zebrafish brain. J. Comp. Neurol. *522*, 2266–2285.
43. Yu, S., Cheng, H., François, M., Qualls-Creekmore, E., Huesing, C., He, Y., Jiang, Y., Gao, H., Xu, Y., Zsombok, A., et al. (2018). Preoptic leptin signaling modulates energy balance independent of body temperature regulation. eLife *7*, e33505. https://doi.org/10.7554/eLife.33505.
44. Handa, T., Sugiyama, T., Islam, T., Johansen, J.P., Yanagawa, Y., McHugh, T.J., and Okamoto, H. (2025). The neural pathway from the superior subpart of the medial habenula to the interpeduncular nucleus suppresses anxiety. Mol. Psychiatry *30*, 3752–3764. https://doi.org/10.1038/s41380-025-02964-8.
45. Ahmadlou, M., Shirazi, M.Y., Zhang, P., Rogers, I.L.M., Dziubek, J., Young, M., and Hofer, S.B. (2025). A subcortical switchboard for perseverative, exploratory and disengaged states. Nature *641*, 151–161. https://doi.org/10.1038/s41586-025-08672-1.
46. Amo, R., Fredes, F., Kinoshita, M., Aoki, R., Aizawa, H., Agetsuma, M., Aoki, T., Shiraki, T., Kakinuma, H., Matsuda, M., et al. (2014). The habenulo-raphe serotonergic circuit encodes an aversive expectation value essential for adaptive active avoidance of danger. Neuron *84*, 1034–1048.
47. Petrucco, L., Lavian, H., Wu, Y.K., Svara, F., Štih, V., and Portugues, R. (2023). Neural dynamics and architecture of the heading direction circuit in zebrafish. Nat. Neurosci. *26*, 765–773.
48. Andalman, A.S., Burns, V.M., Lovett-Barron, M., Broxton, M., Poole, B., Yang, S.J., Grosenick, L., Lerner, T.N., Chen, R., Benster, T., et al. (2019). Neuronal dynamics regulating brain and behavioral state transitions. Cell *177*, 970–985.e20.
49. Palumbo, F., Serneels, B., Pelgrims, R., and Yaksi, E. (2020). The zebrafish dorsolateral habenula is required for updating learned behaviors. Cell Rep. *32*, 108054.
50. Svara, F., Förster, D., Kubo, F., Januszewski, M., Dal Maschio, M., Schubert, P.J., Kornfeld, J., Wanner, A.A., Laurell, E., Denk, W., and Baier, H. (2022). Automated synapse-level reconstruction of neural circuits in the larval zebrafish brain. Nat. Methods *19*, 1357–1366.
51. Hildebrand, D.G.C., Cicconet, M., Torres, R.M., Choi, W., Quan, T.M., Moon, J., Wetzel, A.W., Scott Champion, A., Graham, B.J., Randlett, O., et al. (2017). Whole-brain serial-section electron microscopy in larval zebrafish. Nature *545*, 345–349.
52. Vishwanathan, A., Sood, A., Wu, J., Ramirez, A.D., Yang, R., Kemnitz, N., Ih, D., Turner, N., Lee, K., Tartavull, I., et al. (2024). Predicting modular functions and neural coding of behavior from a synaptic wiring diagram. Nat. Neurosci. *27*, 2443–2454.
53. Wanner, A.A., and Friedrich, R.W. (2020). Whitening of odor representations by the wiring diagram of the olfactory bulb. Nat. Neurosci. *23*, 433–442.
54. Muto, A., Lal, P., Ailani, D., Abe, G., Itoh, M., and Kawakami, K. (2017). Activation of the hypothalamic feeding centre upon visual prey detection. Nat. Commun. *8*, 15029.
55. Lister, J.A., Robertson, C.P., Lepage, T., Johnson, S.L., and Raible, D.W. (1999). nacre encodes a zebrafish microphthalmia-related protein that regulates neural-crest-derived pigment cell fate. Development *126*, 3757–3767.
56. Antinucci, P., Dumitrescu, A., Deleuze, C., Morley, H.J., Leung, K., Hagley, T., Kubo, F., Baier, H., Bianco, I.H., and Wyart, C. (2020). A calibrated optogenetic toolbox of stable zebrafish opsin lines. eLife *9*, e54937. https://doi.org/10.7554/eLife.54937.
57. Portugues, R., and Engert, F. (2011). Adaptive locomotor behavior in larval zebrafish. Front. Syst. Neurosci. *5*, 72.
58. Guizar-Sicairos, M., Thurman, S.T., and Fienup, J.R. (2008). Efficient subpixel image registration algorithms. Opt. Lett. *33*, 156–158.
59. Portugues, R., Feierstein, C.E., Engert, F., and Orger, M.B. (2014). Whole-brain activity maps reveal stereotyped, distributed networks for visuomotor behavior. Neuron *81*, 1328–1343.
60. Bogovic, J.A., Hanslovsky, P., Wong, A., and Saalfeld, S. (2016). Robust registration of calcium images by learned contrast synthesis. In 2016 IEEE 13th International Symposium on Biomedical Imaging (ISBI) (IEEE), pp. 1123–1126.

STAR★METHODS

KEY RESOURCES TABLE

REAGENT or RESOURCE	SOURCE	IDENTIFIER
Chemicals, peptides, and recombinant proteins		
Propranolol	Sigma-aldrich	P0884
Deposited Data		
Processed imaging and behavioral data	this study, zenodo	https://doi.org/10.5281/zenodo.18135842
Experimental models: Organisms/strains		
5-7 days post fertilization; Danio rerio: TgBAC(vGlut2a:Gal4;uas:GCaMP6s; nacre −/−)	Muto,[54] Satou,[23]	13a; nns20Tg
5-7 days post fertilization; Danio rerio: TgBAC(ChaTa:Gal4;uas:GCaMP6s; nacre −/−)	Muto,[54] Förster,.[26]	13a; mpn202Tg
5-7 days post fertilization;Danio rerio: Tg(Th1:Gal4;uas:GCaMP6f; nacre −/−)	Muto,[54] Li, J.[25]	ccu1Tg
5-7 days post fertilization; Danio rerio: Tg(DβH:Gal4;uas:CoChR-GFP; nacre −/−)	Mu,[18]	biu20Tg; jf44Tg
5-7 days post fertilization; Danio rerio: Tg(myl7:CoChR-tdTomato)	this study	N/A (this study)
Software and algorithms		
MATLAB 2021 analysis software	this study	github.com/kjherrera23; https://doi.org/10.5281/zenodo.18135842

EXPERIMENTAL MODEL AND STUDY PARTICIPANT DETAILS

Animal husbandry

All live animal experiments were performed according to protocols approved by Harvard University Institutional Animal Care and Use Committee (IACUC). For all transgenic fish used, crosses were made between adults that were heterozygous carriers of a *mitfa (±)* mutation that generates the *nacre* phenotype.[55] For all experiments, *mitfa* (−/−) null mutations were screened for and utilized. Larvae were housed in an incubator at 28°C with a 14/10 h day/night cycle until 5 days post fertilization (dpf) in filtered facility water). The water in dishes containing embryos was exchanged daily. After 5 dpf, larvae were fed fresh paramecia daily. All experiments were performed on larvae between 5 and 7 dpf. A list of transgenic lines used is provided in the key resources table.

METHOD DETAILS

Transgenic line generation

The tg(myl7:CoChR-tdTomato) line was generated using the tol2 transposase (cite) method. Briefly, gateway cloning (cite) was used to combine a p5e vector containing the 3kb myl7 promoter, a pMe containing CoChR-tdTomato[56] and a p3e containing a poly-A tail. This plasmid was injected into the single-cell staged embryos of tg(vGlut:gal4;uas:GCaMP6S) parents. Embryos were screened for tdTomato expression and propagated.

Heart rate and behavior acquisition

For all behavior and imaging experiments, larvae were embedded in 2% low melting point agarose on 50 mm petri dishes. Following embedding, the fish and agarose were submerged in filtered facility water and allowed to further stabilize for at least 2 h. Approximately 30 min before the experiment began, the agarose surrounding the tail, as well as the rostral tip of the fish were removed to allow for trackable tail movements and chemical stimulus presentation, respectively. Salt stimuli (50 mM NaCl) were presented to the fish using a previously described gravity-driven perfusion system.[20] Visual dark flashes were presented through a 625 nm LED (Thorlabs M625L4) placed above the fish. All stimuli were presented for 10 s, with interstimulus intervals of either 300 s or 60 s.

Tail tracking and heart rate recordings were acquired through a single FLIR Blackfly camera placed below the fish at 100 Hz via infrared illumination (850 nm ThorLabs LED M850L3) presented from above the fish. In the light path between the IR LED and the camera, we placed a 4× objective (AMScope PF4X-INF) to provide enough magnification to visualize the heart. Before the

experiment begins, the center location of the heart is manually selected, and a 20 × 20 pixel image surrounding the heart is saved for further processing every 30 ms. For tail tracking, a tail skeleton consisting of 10 points is automatically detected and saved using a previously described algorithm[57] at every time point (100 hz) during the experiment. Stimulus control, as well as heart and behavior acquisition, were performed using a single custom-written LABVIEW program.

For combined heart-rate and optomotor response experiments, a second preparation was built, with the objective and camera placed above the fish and infrared illumination placed below. This allowed for a projector to be placed below the fish in order to present visual stimuli. To induce fear states, we used the chemical delivery apparatus described above. Square gratings moved either leftward or rightward for up to 8 s every 20 s. To prevent struggles being induced by perceived futility, we stopped the moving gratings after each turn event. To induce heart rate dynamics comparable to the ones generated in the other assays, we presented 10-s pulses of 50 mM salt to the larvae every 6 min.

Whole field motion stimulation

To probe the larvae's visual sensitivity during tachycardia, we presented black and white gratings with a period of 7 mm to the scene directly below the fish using custom-written LabVIEW software. To measure heart rate in these experiments, we placed the recording camera and 4× objective above the fish. Visual gratings moved at 1.5 cm/s either to the left or right every 20 s for up to 8 s. To prevent futility-induced passivity[18] grating motion ceased immediately after the fish attempted a turn as detected by the online tail-tracking software.

Pharmacology

All working solutions were made fresh in filtered fish water the same day of the experiment. Larvae were first incubated in the drug for at least 2 h and then embedded. The embedded larvae were then immersed in the same concentration of drug. Sibling control fish went through the same procedure, but without any drug added to the water.

Calcium imaging

For all functional imaging experiments, we used a custom-built two-photon microscope. Excitation was provided by a femto-second pulsed *Ti:Sapphire laser (MaiTai, Spectra-Physics)* set to 950 nm. The sample at power was <10mW. Frames were acquired at 0.7–1.1 Hz. Microscope control and image acquisition were performed by a single custom-written LABVIEW program. For nodose imaging experiments, larvae were embedded on either their right or left sides. For all other experiments, larvae were embedded dorsal side up.

Optogenetic cardiac pacing experiments

To perform optical pacing concurrent with testing their optomotor response, a slit was cut into the side of a 10 mL Petri dish to allow the cannula of a ThorLabs fiber optic cable (M98L01) to be fixed flush with the floor near the center. The wall was repaired with epoxy. Larvae were embedded such that the output of the fiber-optic cable was even with the posterior side of the heart. A power was identified that did not affect control fish, and still led to cardiac contractions in transgenic fish positive for myl7:CoChR. During pacing sessions where the target frequency was 2 Hz, the LED was on for 200 ms and off for 300 ms. For 2.5 Hz the LED was on and off for 200 ms.

During imaging experiments, we needed to avoid illuminating the fish and recording light from the photomultiplier tube at the same time to prevent photodamage of the PMT. Thus, we used a gated PMT (Hamamatsu H11526-01-NN) for collecting emitted photons, and interleaved recording and stimulation during the galvo scanning, such that during the forward scan, the PMT was on and light source off, and during the backward scan, the light source was on and PMT unpowered. To enable rapid switching between on and off states, we used a blue laser (Coherent OBIS 1178767). This was fed directly to the heart of the fish via a 400 μm fiber optic cannula (CFMLC14L20) - controlled by a manual micromanipulator (Siskiyou SD-130). The pacing stimulation was otherwise the same as for the behavior.

2-Photon ablations

Ablations were performed using a Zeiss LSM 980 NLO Multi-photon microscope. Using the bleaching function, an ROI was drawn around the region and after 10 frames a 5 ms pulse of max power, 850 nm, laser was applied every 10 s until the area of interest was eliminated.

QUANTIFICATION AND STATISTICAL ANALYSIS

Extraction of heart rate and relative fill volume from saved images

To extract heart rate from the 20 × 20 pixel movies saved during all experiments, we used a custom pipeline written in MATLAB. We first performed PCA across time and then examined the first 7 principal components to identify the components with the strongest frequency power in the 1–5 hz band. This signal was assumed to be related to heart rate. We then extracted the time between peaks in this signal using MATLAB's *findpeaks* function and manually selecting a *'MinPeakProminence'* value that sufficiently captured peaks after visual inspection. Peaks detected within 200 ms of the preceding peak were removed. The instantaneous heart rate was then

defined as the inverse of the time between the detected peaks. All fish with a median baseline less than 1 Hz were removed from analysis. The change in luminance from the extracted heart was used to estimate blood flow. The difference was calculated from the peak luminance during the heart beat and the trough. To compare across fish, we normalized by the average change in luminance at 2.4 Hz for threat-related tachycardia, or the average change in luminance across all beats for the pacing experiments.

Image segmentation and registration

Neural signals from within the brain were extracted by first segmenting every imaged plane into 2-dimensional voxels. This was done by first correcting for motion in XY across time[58] and then performing segmentation based upon local correlations of pixel fluorescence across time following a previously described protocol.[20,59] For the sympathetic nervous system - which has relatively few cells - neuronal cell bodies were manually segmented. Registration of functional stacks to a single reference volume was done using the BigWarp plugin in FIJI.[60] Landmarks that connected functionally imaged anatomy to the reference anatomy were selected individually for each experiment.

Identification of heart-rate related cells

To classify neuronal responses we first computed DF/F values, assuming the baseline to be the median fluorescent values. We then specifically selected cells that were "active" above noise by comparing the variance of the frame-by-frame differential of the trace to the overall trace. Cells where this value was greater than 1.2 were deemed to be inactive or noisy, and removed from analysis. We then generated regressors from the heart rate and tail behavior of the animal, as well as the stimuli presented to the animals. Each parameter was convolved with a kernel representing the onset and offset dynamics of GCaMP6S to make these regressors. These regressors were cross-correlated with each neuron's calcium trace. Neurons were defined to be most correlated to a given stimulus when that stimulus generated its greatest correlation *and* the peak correlation coefficient was greater than 0.3.

Cell Reports, Volume *45*

Supplemental information

Synchronization of behavioral and cardiac dynamics in larval zebrafish

Kristian J. Herrera, Arman Zarghani-Shiraz, Misha B. Ahrens, Florian Engert, and Mark C. Fishman

458 ## Supplemental Figures

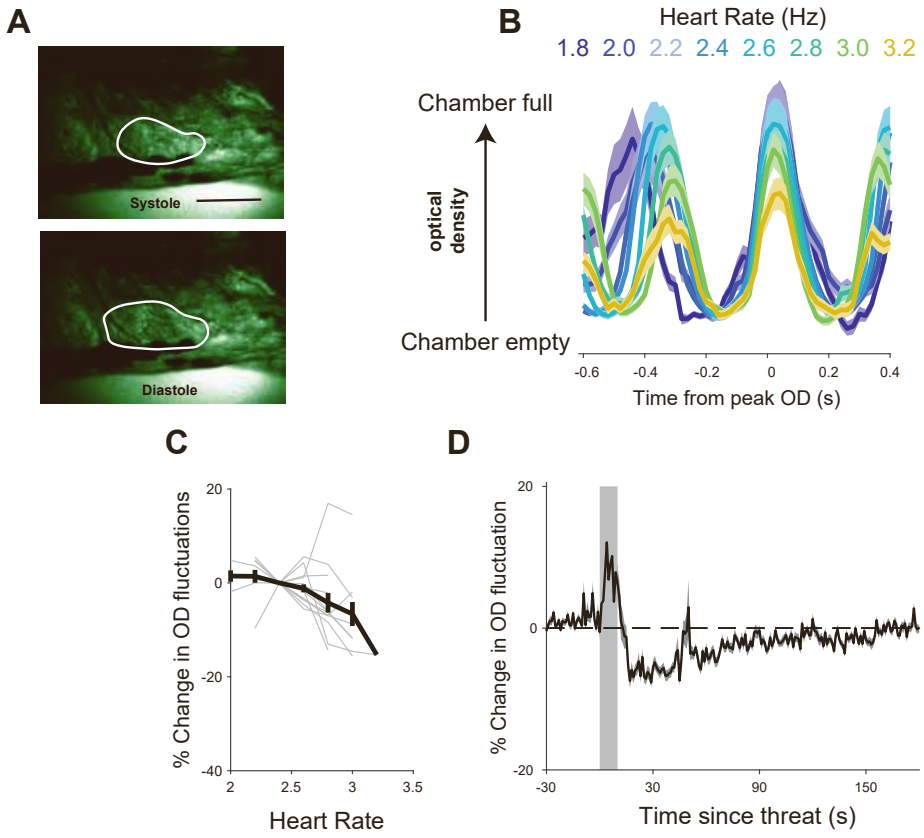

Figure S1. Blood flow is mildly anti-correlated with heart rate (A) Transmitted light image of a sample zebrafish from the side showing systole (top) and diastole (bottom). False colored with FIJI thallium colormap to enhance contrast (white indicates higher transmission). Scale bar 100 μm. (B) Average fluctuation in OD across a heart beat, averaged for all heart beats across fish according to the heart rate Colors from blue to yellow indicate increasing heart rate, with a shrinking magnitude of fluctuations (change in brightness from chamber full to chamber empty) as heart rate increases. (C) Percentage change in magnitude of OD fluctuation (change in brightness from chamber full to chamber empty) as a function of heart rate relative to the average magnitude of OD fluctuations at 2.4 Hz. (D) Percentage change in magnitutde of OD fluctuation after a threat compared to before average before a threat.

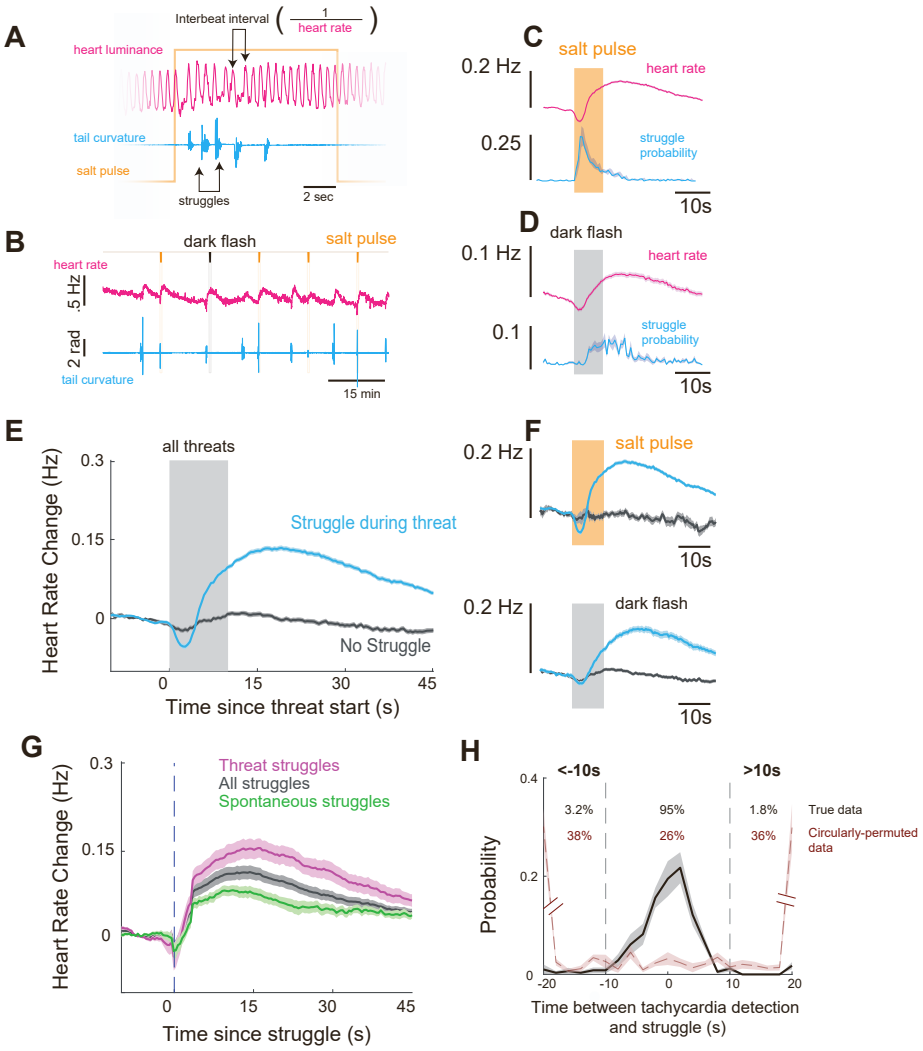

Figure S2. Tachycardia events occur with struggles (A) Sample data from 12 seconds illustrating indvidual heart beats (pink) and tail events (blue) during a threat (salt, orange). (B) Sample experiment showing different threats (darkflash, black, and salt pulse orange), heart rate (pink) and tail (blue) over 30 minutes. (C) Stimulus-triggered heart rate (pink) and tail response probability (blue) following a salt pulse ($p < 0.00001$). (D) Stimulus-triggered heart rate and tail response probability (blue) following a dark flash ($p < 0.00001$). (E) Stimulus triggered heart rate following threats (either dark flash or salt pulse) where the fish struggled during the threat (blue) and those where it did not (gray), showing almost no tachycardia following trials without a struggle. (F) Data in (E) split for salt pulses (top) and dark flashes (bottom). (G) Struggle-triggered heart rate average for all struggles (gray), those that occurred during threats (pink) and those that occurred spontaneously (green). (H) Histogram of the onset of tachycardia events relative to the time of the nearest struggle. Roughly 95% of tachycardia events occur within 10 seconds of a struggle. Events separated greater than or less than 20 or -20 seconds are accumulated in the largest and smallest bins.

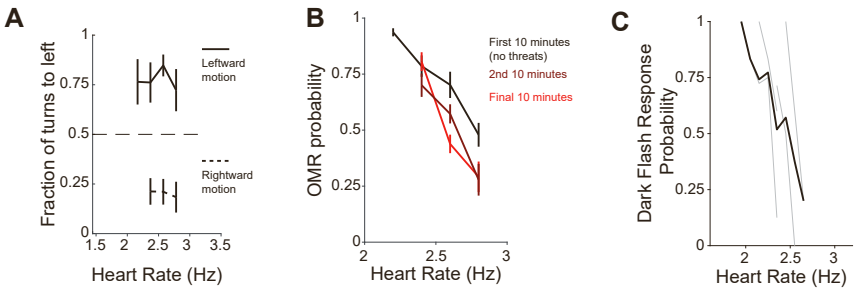

Figure S3. Supporting Material for Figure 1 (A) Probability of the first turn being toward the left as a function of heart rate (x-axis) and whether or not the motion stimulus is to the left (top, solid) or right (bottom, dashed). (B) Probability of responding to OMR trial versus heart rate for data separated into 3 epochs - first 10 minutes (black), during which no salt-pulses are delivered, and the second (brown) and final (red) 10 minutes, during which salt pulses are delivered every 6 minutes. (C) Probability of a struggle response to a 10 second dark flash as a function of heart-rate.

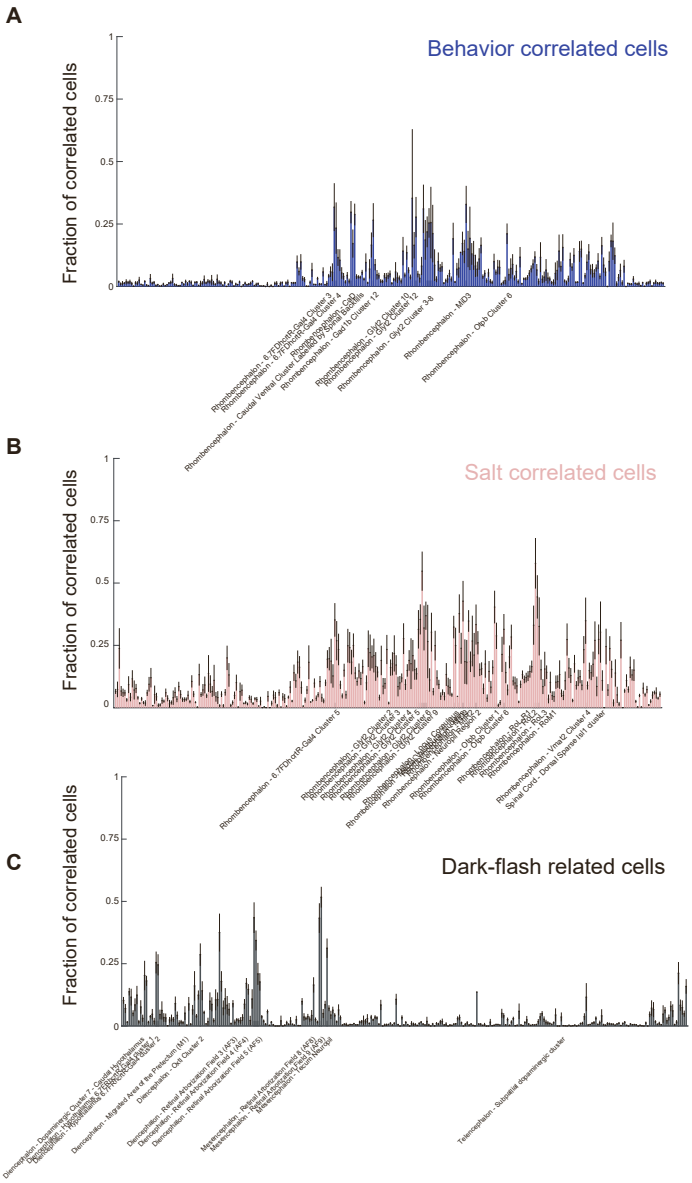

Figure S4. Supporting Material for Figure 2 (A) Fraction of cells in each Z-brain mask with strongest correlation to Behavior (masks with >20% are labeled). (B) Fraction of cells in each Z-brain mask with strongest correlation to salt pulse (masks with >30% are labeled). (C) Fraction of cells in each Z-brain mask with strongest correlation to salt pulse (masks with >20% are labeled).

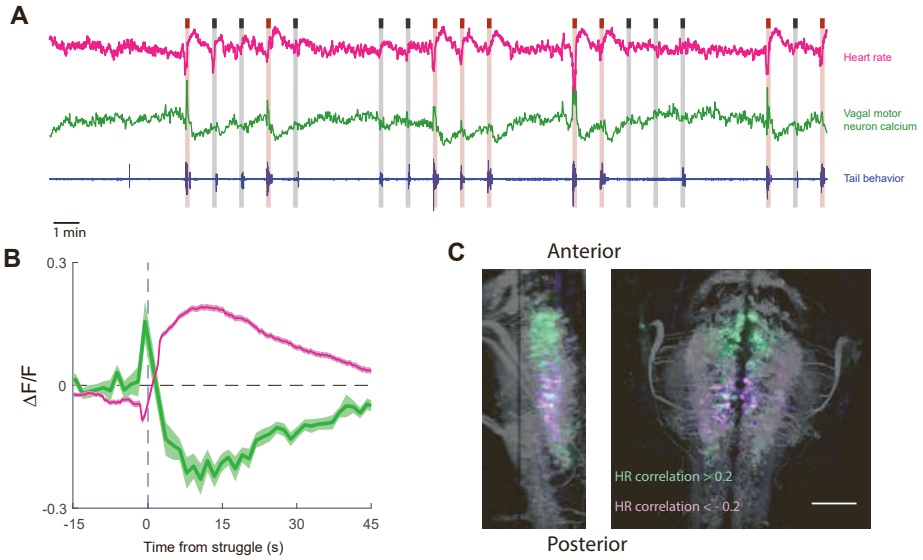

Figure S5. Heart rate anticorrelated activity in vagal motor neuron reflects bradycardia and tachycardia (A) Example trace from a heart-rate anticorrelated cell in the motor vagus region. (B) Struggle-triggered average of all heart-rate anticorrelated cells (green) from 11 fish plotted against average struggle-triggered heart rate. (C) Map of heart rate correlated (green) and anti-correlated (pink) activity in the motor vagus, generated from registering correlations from all 11 fish to a single reference image. Left image shows the vagus nucleus from the side, right image shows a dorsal view. scale bar 50 μm.

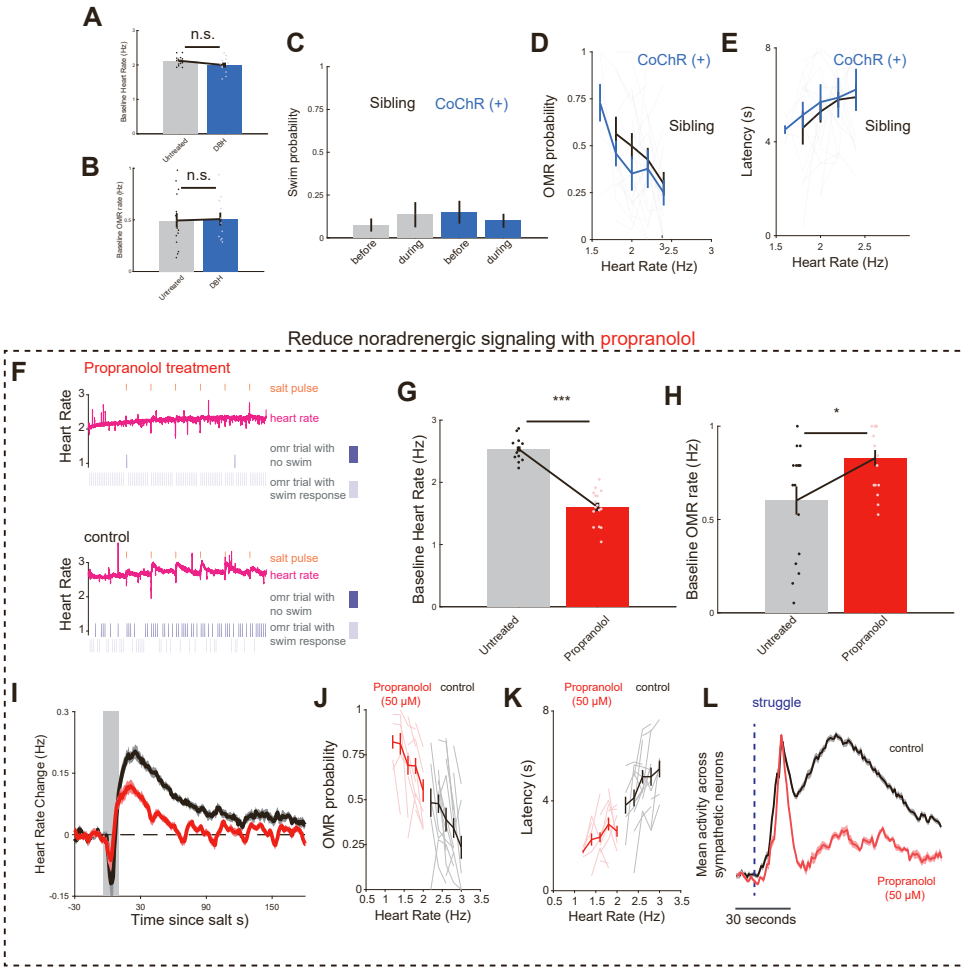

Figure S6. Heart rate anticorrelated activity in vagal motor neuron reflects bradycardia and tachycardia (A) Baseline heart rate, from first 10 minutes of experiment, for *DβH:CoChR-eGFP* expressing larvae (blue) and sibling controls (gray). p = 0.1772, wilcoxon ranksum. (B) Baseline optomotor response rate, from first 10 minutes of experiment, for DβH:CoChR-eGFP expressing larvae (blue) and sibling controls (gray). p = 0.9173, wilcoxon rank sum. (C) Probability of a struggle during the 30 seconds before or 30 seconds during illumination with blue light for *DβH:CoChR-eGFP* expressing larvae (blue) and sibling controls (gray). (D) OMR probability as a function of heart rate for *DβH:CoChR-eGFP* expressing larvae (blue) and sibling controls (gray). (E) OMR response latency for *DβH:CoChR-eGFP* expressing larvae (blue) and sibling controls (gray). (F) Sample experiment recording heart rate and OMR performance (see Figure 1C) in a fish treated with 50 μM propranolol (top) and a sibling control (Bottom). (G) Baseline heart rate, from first 10 minutes of experiment, for larvae treated with propranolol (red) and sibling controls (gray). p = 1.54106, wilcoxon rank sum. (H) Baseline optomotor response probability, from first 10 minutes of experiment, for larvae treated with propranolol (red) and sibling controls (gray). p = 0.0210, wilcoxon rank sum. (I) Stimulus-triggered heart rate for fish treated with propranolol (red) and sibling controls (black) following a salt pulse. (J) Relationship between heart rate and probability to perform OMR by fish treated with 50 μM propranolol (n = 13) and sibling controls (n = 15). Light lines indicate individual fish. Error bars are SEM. (K) Relationship between heart rate and latency to first swim during OMR trial by fish treated with 50 μM propranolol (n = 13) and sibling controls (n = 15). Light gray lines indicate individual fish. Error bars are SEM. (L) Struggle-triggered (dashed blue line) calcium activity averaged all neurons in the sympathetic ganglia for control fish (black, n = 4 fish) and fish treated with propranolol (red, n = 3 fish)

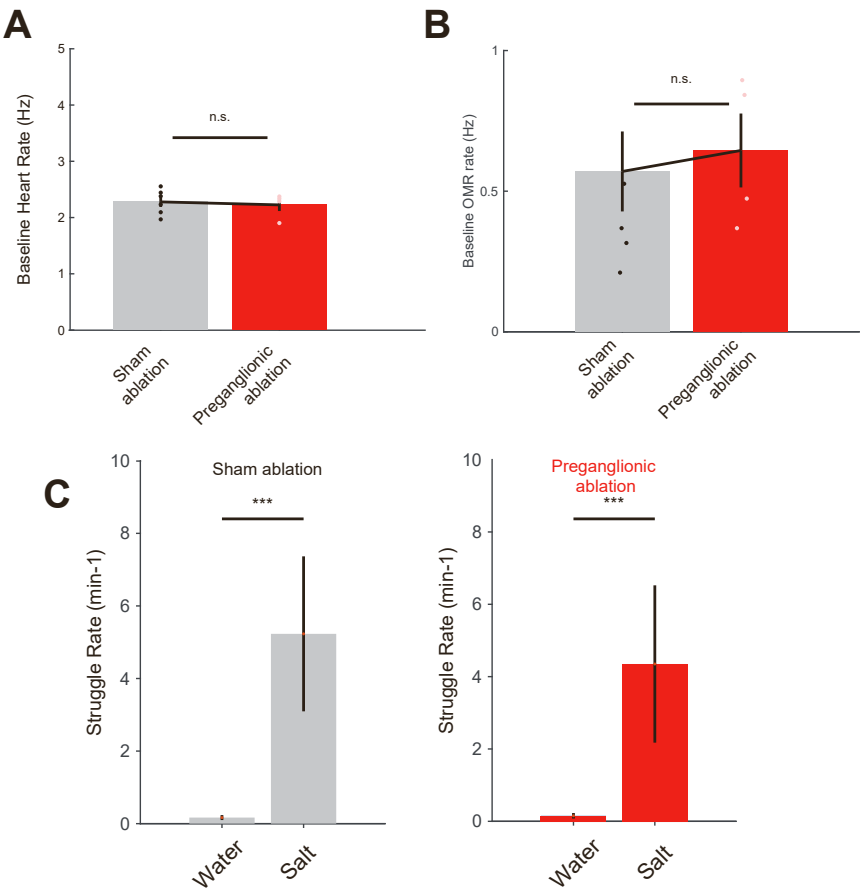

Figure S7. Supporting Material for Figure 3 (A) Baseline heart rate, from first 10 minutes of experiment, for larvae treated with propranolol (red) and sibling controls (gray). p = 0.6095, wilcoxon rank sum. (B) Baseline optomotor response probability, from first 10 minutes of experiment, for larvae treated with propranolol (red) and sibling controls (gray). p = 0.8190, wilcoxon rank sum. (C) Struggle rate (number of detected struggles per minute) while fish is exposed to water or salt for control sham ablations (paired t-test, p = 0.000128) and fish with preganlionic ablations (paired t-test, p = 0.000645).

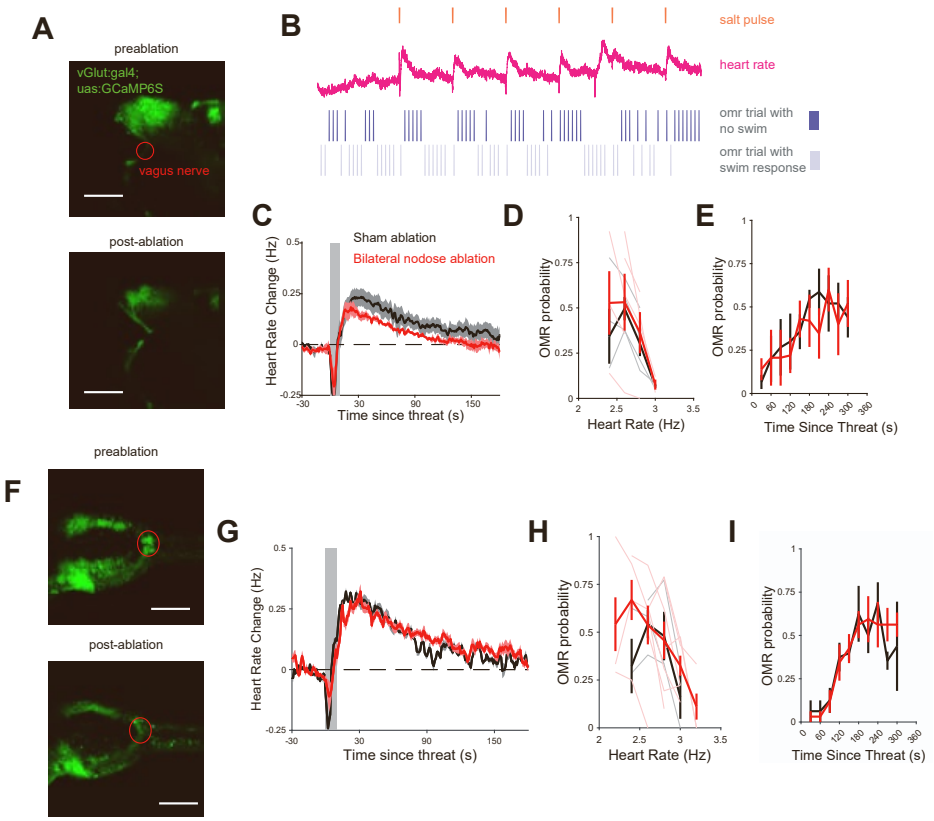

Figure S8. Supporting Material for Figure 1 (A) Projections of confocal stack of *vGlut2a:gal4;uas:GCaMP6s* fish imaged from the side before and after severing of the vagus nerve. scale bar (150 µm). (B) Heart rate (red), salt stimulus, and optomotor response (blue) from fish shown in (A). (C) Stimulus triggered average heart rate response to salt in control and bilateral vagus nerve ablations. (D) Probability of responding to sideways moving gratings for sham ablation of non-vagal neurons (black) and bilateral vagus nerve ablations (red). (E) Probability of optomotor response as a function of time lapsed since threat following sham-ablation of non-vagal neurons (black) and bilateral vagus nerve ablations (red). (F) Projections of confocal stack of vGlut2a:gal4;uas:GCaMP6s fish imaged from the top before (top) and after (bottom) lesioning the area postrema. scale bar (150 µm). (G) Stimulus triggered average heart rate response to salt in control and area postrema ablations. (H) Probability of responding to sidways moving gratings for sham ablation of non-vagal neurons (black) and area postrema ablations (red). (I) Probability of optomotor response as a function of time lapsed since threat following sham-ablation of non-vagal neurons (black) and area postrema ablations (red).

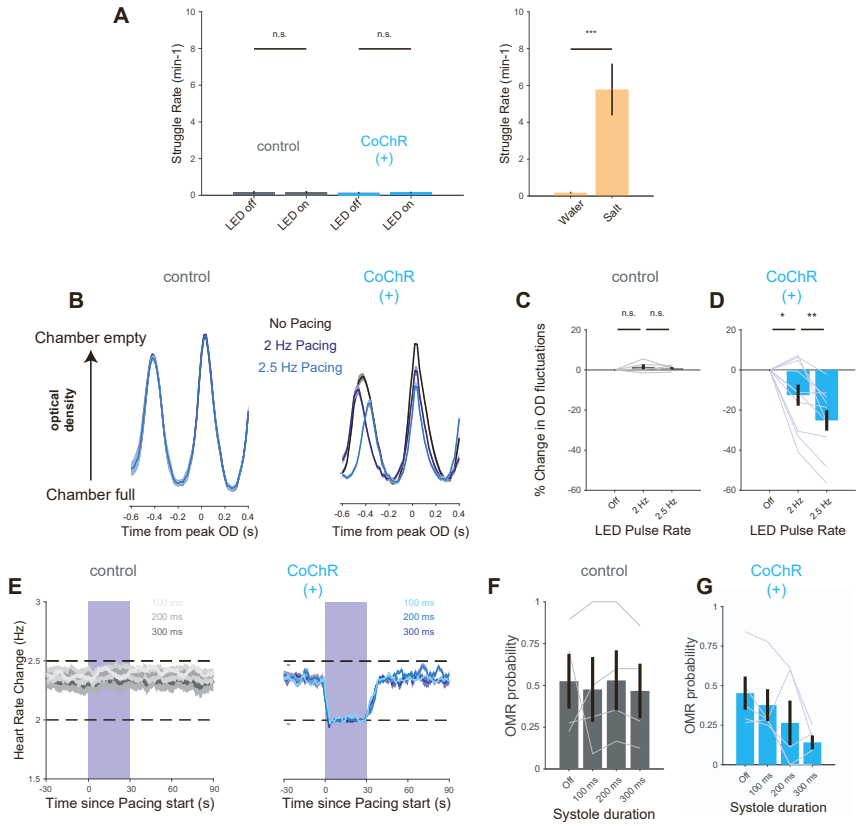

Figure S9. Supporting Material for Figure 5 (A) Struggle rate (number of detected struggles per minute) while the LED is off or being paced. Neither controls nor fish expressing CoChR show increased struggles after LED is turned on (paired t-test, p = 0.9540, control; p = 0.8548, CoChR-expressing). As a comparison, struggle rate is significantly increased during salt exposure from Figure 1 (p = 0.00022). (B) Average optical density change during heart beats, calculated as 1-luminance in the heart, triggered (t = 0) around the lowest luminance. Lower values indicate expanded chamber, and thus correspond to diastole. OD values are normalized to luminance at the detected peak - which represents systole. Left shows different heart beat types (normal, LED pacing at 2 and 2.5Hz) for controls, while the right shows the same for *myl7:CoChR-tdTomato* fish. (C) Average percent fluctuation of OD across a heart beat relative to heart beats when the LED is off in control fish where no change in inferred volume is seen (paired t-test, no pace > 2 Hz, p = 0.5601; 2 Hz > 2.5 Hz, p = 0.27). (D) Average percent fluctuation of OD across a heart beat relative to heart beats when the LED is off in *myl7:CoChR-tdTomato* fish where pacing introduces significant changes in inferred fill volume (paired t-test, no pace > 2 Hz, p = 0.0495; 2 Hz > 2.5 Hz, p = 0.003). (E) Left : average time course of heart rate centered on onset of 2 Hz pacing for tdTomato(-) sibling control fish (gray). for different durations of LED pulses lengths. Shaded area indicates SEM. Right: average heart rate before and during pacing for the myl7:CoChR-tdTomato fish across different LED pulse lengths while pacing. (F) Relationship between optical pacing at 2 Hz with different systole duration as defined by the time within each "beat" where the LED is kept on (100-300 ms) and probability to perform OMR in sibling controls (gray, n = 4). Error bars are SEM. (G) Relationship between optical pacing at 2 Hz with different systole duration as defined by the time within each "beat" where the LED is kept on (100-300 ms) and probability to perform OMR in *myl7:CoChR-tdTomato* fish (gray, n = 5).